Tides on Other Earths: Implications for Exoplanet and Palaeo-Tidal Simulations

Blackledge, Benedict; Green, Mattias; Barnes, Rory ; Way, Michael

Geophysical Research Letters

DOI:
10.1029/2019GL085746

Published: 28/06/2020

Peer reviewed version

Tides on other Earths: implications for exoplanet and palaeo-tidal simulations

B. W. Blackledge[1], J. A. M. Green[1], R. Barnes[2], and M. J. Way[345]

[1]School of Ocean Sciences, Bangor University, Menai Bridge, UK
[2]Department of Astronomy, University of Washington, Seattle, Wa, USA
[3]NASA Goddard Institute for Space Studies, New York, USA
[4]Goddard Space Flight Center Sellers Exoplanet Environments Collaboration
[5]Theoretical Astrophysics, Department of Physics and Astronomy, Uppsala University, Uppsala, Sweden

Key Points:

- The possible tidal dissipation rates on Earth can span at least 3 orders of magnitude, with bathymetry this range narrows.
- Geologic features currently unique to Earth are crucial factors in the tidal energy budget.
- Time varying dissipation due to surface evolution such as tectonics should be considered in models of evolving planetary rotation.

Corresponding author: Dr J. A. M. Green, `m.green@bangor.ac.uk`

Abstract

A key controller of a planet's rotational evolution, and hence habitability, is tidal dissipation, which on Earth is dominated by the ocean tides. Because exoplanet or deep-time Earth topographies are unknown, a statistical ensemble is used to constrain possible tidal dissipation rates on Earth and similar ecoplanets. A dedicated tidal model is used together with 120 random continental configurations to simulate Earth's semi-diurnal lunar tide. The results show a possible ocean tidal dissipation range spanning 3 orders of magnitude, between 2.3GW–1.9TW (1TW=10^{12}W). When model resolution is considered, this compares well with theoretical limits derived for the energetics of Earth's present day deep-ocean-only environment. Consequently, continents exert a fundamental control on tidal dissipation rates and we suggest that if plate tectonics are present on a planet it will induce a time-varying dissipation analogous to Earth's. This will alter rotational periods over millions of years and further complicate the role of tides for planetary evolution.

Plain Language Summary

The daylength of a planet is key for habitability because it regulates the rate with which solar radiation is received and redistributed at the surface. A main controller of a planet's daylength is the ocean tide, because the dissipation of tidal energy works as a brake on the planet's spin, increasing the daylength. Tides are sensitive to the continental arrangement on a planet, but there are no details of the surface of any exoplanet and only limited information of what Earth looked like in the distant past. The change in Earth's daylength forces the Moon to recede into a higher orbit, but the present-day recession rate is very high and doesn't fit our age models of the moon, implying the tides must have been much weaker in the distant past. Here, we use a series of tidal predictions for random continental configurations of Earth to provide a range of tidal dissipation rates and thus an estimate of how the tides in the deep past may have evolved as Earth's continents grew more and more complex. This research also provides a range of dissipation rates that can be used for simulations of the rotational and orbital evolution of exoplanets.

1 Introduction

The ocean tides drive and influence a range of geophysical processes. The tidal energy dissipated in shallow waters controls shelf sea stratification (Simpson et al., 1990) and sustains a vertical nutrient flux vital for marine primary productivity in shallow and deep environments (Hickman et al., 2012; Williams et al., 2018; Tuerena et al., 2019). In the deep ocean, tidally driven mixing is integral to the global overturning circulation (Kuhlbrodt et al., 2007; Srokosz et al., 2012; Wunsch & Ferrari, 2004), whereas the tidal range during particular geologic periods may exert an influence on the evolution of complex life (Balbus, 2014). The tides are also a first-order control on orbital evolution for the Earth-Moon system (Bills & Ray, 1999; Munk, 1968). This is illustrated through the current, anomalously high, (3.8cm yr^{-1}) recession rate of the Moon which does not match its radiometric age of 4.5 Gyr (Dickey et al., 1994; Barnes, 2017). The erroneous assumption of a constant modern globally integrated dissipation rate suggests an Earth-Moon system age of about 1.5 Gyr (Darwin, 1899; MacDonald, 1964; Munk, 1968). The missing factor may be the time-varying effect of the continental configuration on the tide, a condition shown to have driven long-term dissipation variability on Earth (Kagan, 1997; Green et al., 2017). Consequently, the implications of an ocean tide controlled by a planets' continental configuration is an important parameter when modelling the orbital evolution of an ocean bearing planet.

To date, there are over 4000 confirmed exoplanets, of which more than 630 are in multi-planet systems (see http://exoplanet.eu/catalog/ for the latest estimate). The masses

of these planets range from gas giants of the order of ∼1000 $M_\oplus$ (Earth masses), to less massive objects that are often characterised as terrestrial planets, thought to be similar in composition and scale to the terrestrial planets in our solar system (exoplanets.eu). Concurrently, attempts have been made to estimate the 'habitability' of these planets, a condition based on the probability of a given planet being able to support liquid water at its surface (Kasting et al., 1993) – one of many definitions for habitability. This is a function of host star irradiance, planet-star separation and the chemical composition of the planet and its climate system (Seager, 2013). These conditions determine the extent of the Habitable Zone, the theoretical shell around a given star at which liquid water could exist, given the appropriate climatic conditions (Kopparapu et al., 2013).

As the number of confirmed planets has grown, planets with potential oceans emerge (e.g., Tsiaras et al., 2019), and the number of planets that appear to be within their habitable zone is expected to increase (Batalha et al., 2013). Estimates put the number of planets in the Milky Way as high as $\sim 10^{10}$ (Dressing & Charbonneau, 2015). Since smaller, potentially terrestrial, planets far outnumber the larger gaseous planets (Cassan et al., 2012; Howard, 2013; Fressin et al., 2013), habitable planets may be common.

Little is known about these planets, which has led to the widespread use of numerical models of potential climatic conditions to determine a probability of a given body hosting water (Seager, 2013), but there are large uncertainties in this approach. For example, varying host-star irradiances and masses, and planetary atmospheric compositions, masses, rotation rates, eccentricities, and obliquities will drastically alter the conditions at the surface (Kasting et al., 1993; Williams & Pollard, 2002, 2003; Yang et al., 2014; Way et al., 2016; Way & Georgakarakos, 2017; Way et al., 2018; Colose et al., 2019). Few of these simulations, however, consider the effect of a water ocean tide, despite tidal friction being a key controller on orbital evolution, and hence habitability (Bills & Ray, 1999; Lingam & Loeb, 2018; Egbert et al., 2004; Green et al., 2019).

If a planet's spin frequency is greater than its moon's orbital frequency, tidal friction will increase the semi-major axis length and rotational period of the planet, leading to a transfer of angular momentum due to the torques exerted on the body (Darwin, 1899). This process leads to an increase of the angular momentum of the tide raiser and a decrease in the planet's rotation rate, so the rotational evolution depends on the amount of tidal energy dissipation. This is in turn a function of the height of the tidal bulges and the rheology of the planet's interior (Renaud & Henning, 2017), including the fraction of water on it. On Earth today, the solid body dissipation for the dominating M_2 lunar tide is 0.08TW (Ray et al., 1996), whereas the associated total ocean tidal dissipation rate is 2.4TW (Egbert & Ray, 2001). Obviously, a liquid ocean can provide a more energetic tidal response than a solid body alone because it is easier to excite a tide in the ocean than in the solid Earth.

There are links between a planet's potential habitability and its rotation rate, e.g., full spin-orbit synchronization at lower rates and the reduction of meridional atmospheric convection at higher rotation rates due to a stronger Coriolis force (Yang et al., 2014). To properly constrain a planet's climatology, and therefore habitability, a range of variables, including the rotation rate, topography and land/ocean mask, must be known (Yang et al., 2014; Way et al., 2016; Way & Del Genio, 2019; Colose et al., 2019). So a planet's past, present and future total tidal dissipation rate must be quantified, to improve estimates of those other dependent properties.

Here, we constrain the potential range of tidal dissipation on an Earth-like planet using a dedicated numerical tidal model and a large sample of random continental configurations. This will allow us to produce bounds on the potential dissipation rates that can then be used for rotational evolution simulations, and to provide error bounds on simulations of deep-time tides when Earth's surface looked very different from today's.

2 Methods

We use OTIS, the Oregon State University Tidal Inversion Software, a well established numerical tidal model that has been used to simulate deep-time past, present and future tides on Earth (Egbert et al., 2004; Green et al., 2017, 2018; Wilmes et al., 2017), and on ancient Venus (Green et al., 2019). The model has been bench-marked against other global non-assimilating tidal models and demonstrated to reproduce Earth's present day tide with a high degree of accuracy (Stammer et al., 2014). It solves the linearised shallow-water equations,

$$\frac{\partial \mathbf{U}}{\partial t} + f \times \mathbf{U} = -gH\nabla(\eta - \eta_{EQ} - \eta_{SAL}) - F, \quad (1)$$

$$\frac{\partial \eta}{\partial t} = -\nabla \cdot \mathbf{U} \quad (2)$$

where $\mathbf{U}$ is the depth integrated volume transport (the current velocity u times the depth H), g is the gravitational constant, $\mathbf{f}$ the Coriolis vector, ζ is the tidal amplitude. η_{SAL} is the elevation due to self-attraction and loading (SAL; here set to 8% of the amplitude following Ray (1997)) and η_{EQ} the equilibrium tidal elevation. The model is forced by the astronomical tide generated by the Lunar and Solar gravitational potential. $\mathbf{F} = \mathbf{F}_B + \mathbf{F}_w$ is the total loss of energy to bed friction (F_B) and tidal conversion (F_w, describing the generation of an internal tide). The scalar product $\mathbf{F}\cdot\mathbf{u}$ thus gives the tidal dissipation rate, D. Bed friction is given by

$$\mathbf{F_B} = C_d \mathbf{u}|\mathbf{u}| \quad (3)$$

The drag coefficient, C_d=0.003, represents mean seabed roughness and is based on an appropriate value for present day Earth (see, e.g., Taylor, 1920), and $\mathbf{u}$ is the combined velocity vector of all the tidal constituents. Note that the model is insensitive to the chosen value of C_d, and sensitivity simulations (not shown) with it varying by a factor 3 did not significantly change the results. However, this may not be the case for aqua-planets (no continents), where the dissipation may scale directly with C_d due to a lack of topography. Futhermore, for Earth-like ocean with fine sediments we do not expect C_d to vary beyond this parameter range.

Tidal conversion is important in simulations with topography, and is given by $F_w = C|\mathbf{U}|$, where C is the conversion coefficient given by (Zaron & Egbert, 2006):

$$C(x,y) = \gamma \frac{(\nabla H)^2 N_b \overline{N}}{8\pi^2 \omega}. \quad (4)$$

Here, γ=50 is a scaling factor, N_b is the buoyancy frequency at the seabed, $\overline{N}$ is the average buoyancy frequency in the vertical, and ω is the frequency of the constituent under investigation. Given the surface properties of exoplanets are unknown, the buoyancy frequency is computed from a statistical fit based on observations from present day Earth, or $N(x,y) = 0.00524\exp(-z/1300)$, where z is the vertical coordinate, and the constants 0.00524 and 1300 have units of s^{-1} and m, respectively. Tidal conversion will differ for other fluids (ie: liquid Methane), but we assume a water ocean here.

All simulations were performed for three dominating tidal constituents, but we focus our discussion on those representing the principal semi-diurnal lunar (M_2) and solar (S_2) tides. Their respective constituent periods for Earth today are 12.42, 12 and 23.93 hours. Note that OTIS handles tides only; there is no other forcing included in the model and although inertial oscillations are present we only discuss the ocean tides here.

2.1 Continental configurations and sensitivity simulations

The model grids were generated using Planet Generator (`https://topps.diku.dk/torbenm/maps.msp`), a fractal map generator capable of simulating complex planet sur-

face features, which is feasible because the shape and distribution of continents are approximately fractal-like in nature (Goodchild & Mark, 1987; Mandelbrot, 1982). The generator produces grey-scale images, where each pixel value is between 1 (white) and 0 (black). Here, the images were 360×180 pixels in size, and a flat-bottomed 'bath-tub' ocean grid, at a horizontal resolution of $1^\circ \times 1^\circ$, was built by allocating a depth of 4500 m to all grey-scale pixels with a value below 0.2. The aim here is to evaluate the effect of the position and complexity of the continents on the tide, and a further series of sensitivity simulations on the boundary values was performed, with the coastline at grey-scale values of 0.1 and 0.4, as well as simulations with bottom topography (see below).

In total, 120 different continental configurations were evaluated, including an equilibrium tide simulation without continents (See Table in Supplementary Material for a summary of all the simulations). As each configuration is unique, all configurations are independent of one another, so their general geometry and relative positions are heterogeneous. This represents (to some degree) the variation that would be expected between planets, and between geological epochs on the same planet.To show the total effect of continent size, ocean basin size and coastal complexity, we use the non-dimensional value $R = L_{tot}/\sqrt{A_{ocean}}$. L_{tot} is the total coastline length (km) and A_{ocean} (km^2) is the total ocean area. L_{tot} was found by identifying the coordinates of the coastal boundary between individual continents and the ocean. The distance between neighbouring coordinates were then calculated using a Great-circle technique: the coastal length for each continent was found, and the total global distance was the sum of these values. This is justified as there is little point considering distances smaller than the smallest horizontal resolution in the grid, although Earths' real tides are influenced by small, non-random topographic features.

We also completed two sets of simulations with ocean bathymetry for 8 maps selected from the population (see below). The first has a set global average depth (SGAD) whereas the second set had a set maximum depth (SMD). Both were computed by multiplying the grey-scale values with a constant. It was equal to 4500 for the SMD, so the deepest point will be 4500m and the shallowest 900 m. The SGAD constant was individually chosen so the mean depth of the ocean was 4500m. This gave a maximum depth between 9500–42000m depending on the configuration. Depths of tens of kilometres, for a planet of Earth's radius, is approaching the limit of the shallow-water approximation employed in OTIS. The simulations are summarised in SM Table 1; note that the extreme cases are not discussed further.

These 8 maps, with bathymetry, were also used to test the sensitivity to stratification through simulations with enhanced ($\gamma = 500$ in Eq. (4)) or reduced stratification (using $\gamma = 5$). The 8 maps, but with bathtub bathymetry, were also subject to tests of the effect of the planet's rotation rate by adjusting Earth's day length to 3 hours and 8 days respectively, so that the new M_2 periods are 1.51 and 124.20 hours. Only Earth's rotation period is changed, no adjustment is made to the Lunar period of 27.3 days. Note that a rotation period of 8 days still puts the planet within the fast-rotator regime of its climate dynamics (Way et al., 2018).

2.2 Present Day Earth sensitivity simulations

Three simulations were run for present day Earth. The control used present day ocean bathymetry, the first of two sensitivity simulations had a bathtub ocean with the depth set to 4500m everywhere (see Fig. SM1a–b), whereas the second had Earths' shelf seas removed by setting any ocean initially shallower than 1000m to 1800m to highlight the importance of shelf dissipation. In the control, at the low resolution of $1^\circ \times 1^\circ$, OTIS overestimates the M_2 dissipation rate by a factor 2.5 compared to observed dissipation rates [Egbert and Ray (2001); see our Fig. SM1], whereas S_2 is overestimated by a factor 3. The bathtub configuration is far less dissipative (Fig. SM1b,c) and underestimates

the M_2 and S_2 dissipation rates by factors 25 and 200 respectively. Removing shelf seas gives 0.77TW of M_2 dissipation, compared to the 6.3TW of the control. These results make sense dynamically. In a coarse-resolution simulation not enough energy dissipates in the deep ocean due to underrepresented topography. Because the tidal energy is not lost in the deep ocean, the shelf sea currents are overestimated and, with frictional losses being proportional to the cube of the speed, the dissipation is overestimated. The same happens in the bathtub runs, but there is then no shelf to dissipate the energy on, and instead the global rate drops to deep abyssal values. The stratification sensitivity tests can be found in the SM.

3 Results

3.1 Dissipation

As anticipated, the addition of continents of increasing complexity generates a more energetic tide, highlighted for the eight examples in Fig. 1 and summarised in Fig. 2; these are labelled A–H in the following and chosen because they cover the parameter space in Fig. 2. The globally integrated dissipation in Fig. 2a scales with the magnitude of continental configuration complexity, quantified here as a ratio, R, between the coastline length and the ocean basin area. As R increases, the M_2 tidal dissipation rate follows and soon reaches values two orders of magnitude larger than the rate in the equilibrium tide (i.e., the 2.3 GW at $R = 0$). The dissipation range for a certain value of R can span nearly an order of magnitude, but 36% of the configurations occur within the 0.1–1 TW range. The S_2 response is generally weak (not shown), with an amplitude of about 45% of M_2, although some configurations produce an S_2 dissipation that is larger than M_2 because of S_2 resonances, e.g., configuration E.

Both M_2 and S_2 reach dissipation maxima at continental distributions which are qualitatively among the most fragmentary, with several small scale topographic features introducing local flow acceleration. For M_2, the largest dissipation rate is 1.9 TW (Fig. 1E), while S_2 peaks at 0.67 TW – values 19 and 260 times larger than in our bathtub Earth simulation and on par with the observed dissipation rates on Earth today (Egbert & Ray, 2001). As the coastline length continues to grow (i.e., R increases), the continent area must also increase. This limits the total ocean area and therefore the potential for large integrated tidal dissipation rates as there is a smaller ocean to dissipate energy in. In the extreme case, we have a planet with a large number of basins too small to host a tide. Thus, as R increases, we can expect dissipation to reduce, such as on a surface with many disconnected basins, smaller than usual in our ensemble. This form was not explicitly tested, but it would have quiescent tides under the conditions we use, potentially expanding this range to a greater number of orders of magnitude. We leave exploration of this limit to future work.

There is not a specific configuration, quantified by R, that is especially dissipative; two configurations can have similar R-values, but be qualitatively dissimilar in the actual position of the landmasses (e.g., see configurations D and E in Fig. 1). Given that global dissipation rates are dependent on oceanic area, a configuration that elevates dissipation closer to the equator should result in a larger global value than one with a continent of the same shape at higher latitudes. However, a number of the simulations possess a polar ocean, e.g. H, or in some cases a single large hemispheric ocean with a large tide. The dissipation in these instances can have a large deviation from what could be expected, demonstrated in the increasing variability above very small R-values.

On present day Earth, deep ocean tidal dissipation is driven by conversion at bathymetric features (Egbert & Ray, 2001). The SMD configurations generally have an enhanced dissipation (see Figure 2b) influenced by the continental configuration. The two sets – bathtub and SMD – are significantly different ($F_{1,119} = 0.49$, $p < 0.05$), with the

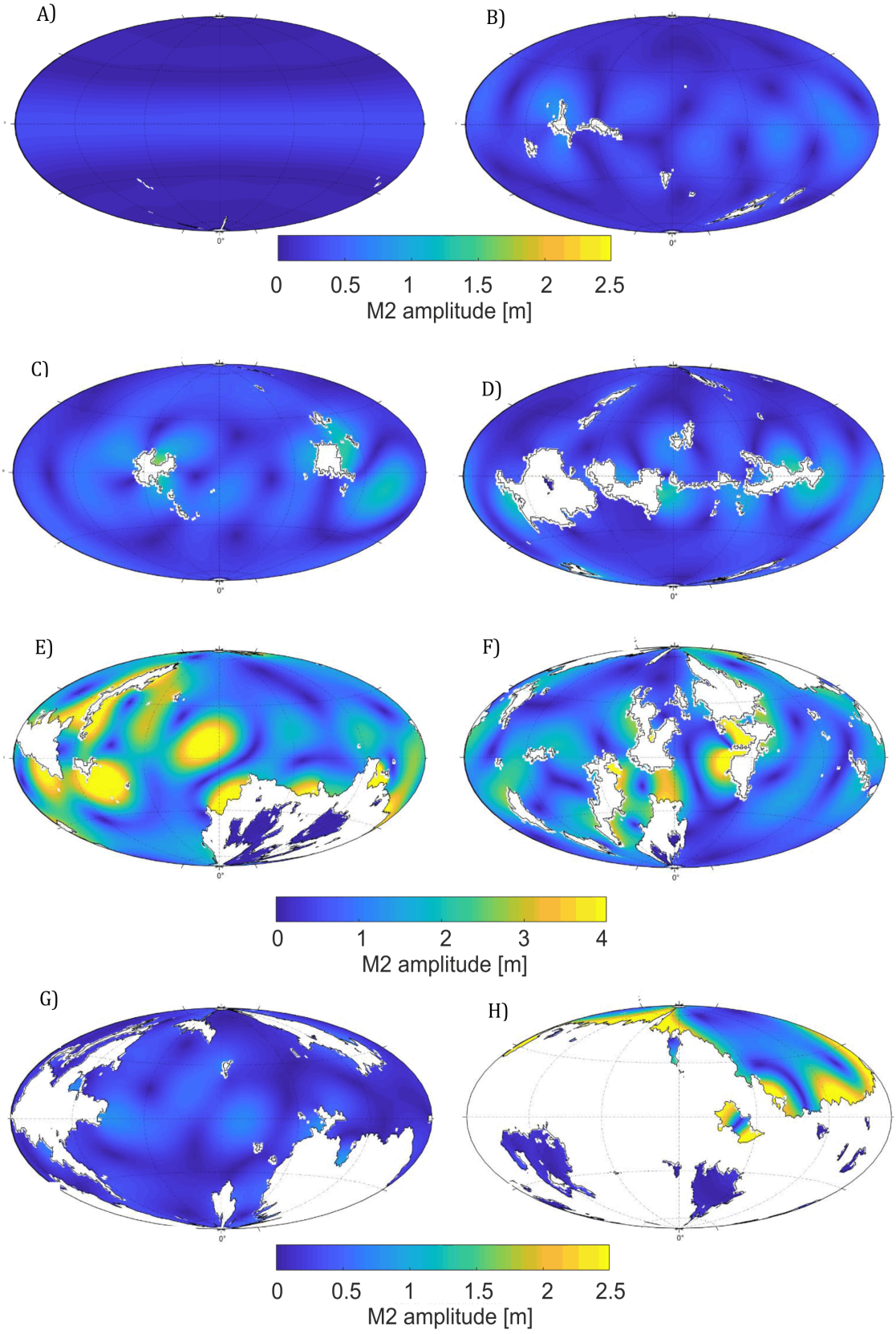

Figure 1. M_2 Tidal amplitudes for the eight selected configurations, A–H. Note the use of two different colour scales: E and F use the second scale, whereas A–D and G–H use the first (which is repeated under panels G–H).

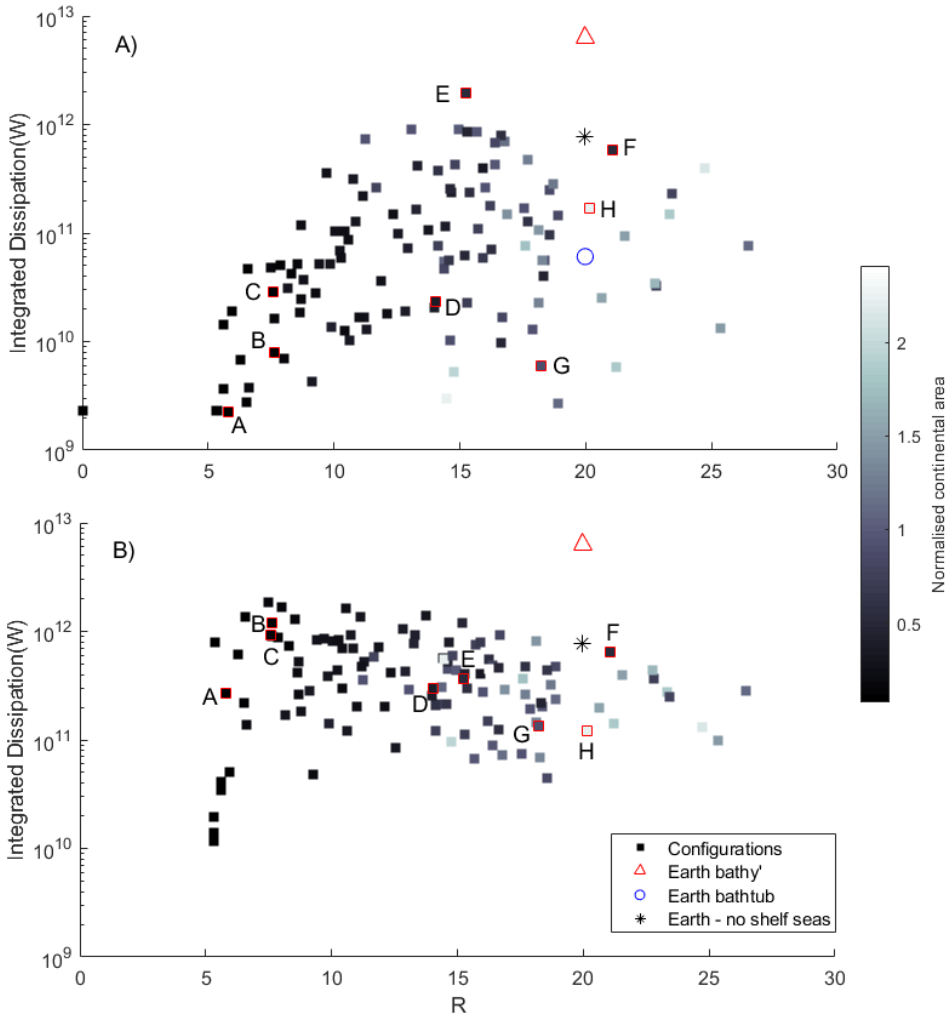

Figure 2. **A)** R versus the globally integrated dissipation rate, D. Note the selected 8 configurations, labelled A–H, outlined in red. The point at R=0 is the control water-world, the Earth controls are shown as a circle (bathtub), triangle (with bathymetry), and the star is Earth without shelf seas. The colour scale of continent area has been normalised against Earth's present continental area of 5.1×10^7 km^2. Additional sensitivity simulations can be found in Table S1. Surfaces with some large number of small disconnected basins were not tested **B)** The same configurations, with a form of random bathymetry, Earth without shelf seas and the control are included for comparison.

bathtub dissipation values being poor predictors of the SMD values. The greatest increases are amongst the configurations that were the least energetic without bathymetry, while the bathtub maximum of 1.83TW can be achieved with smaller and less complex continents. Because our results span 3 orders of magnitude, any upper limit on Earth's deep ocean dissipation remains highly uncertain, however as our ensemble maxima are 1.83TW and 1.92TW, such a limit may lie close to these values at this resolution. While the variance is large ($s^2 = 7.24 \times 10^{10}$ TW^2), adding bathymetry narrows the range of dissipation values compared to the runs without: 92% occur within one standard deviation (0.39TW) of their mean (0.46TW) with bathymetry, as opposed to 76% without bathymetry, although this still spans two orders of magnitude.

3.2 Sensitivity simulations

In the SGAD set, the dissipation rises three orders of magnitude at the lowest R-value (see Table 1 SM). A consistent feature in these simulations is the convergence towards a common dissipation value as the stratification is strengthened by a factor of 10: the most energetic configurations are dampened whereas those at the scatter's lower bound are enhanced. In the SMD set, shown in Fig 2b, the trend is similar, however the dissipation shows less variability within the R scale, while the examples lose their dependence on R. The spatial distribution of the SMD runs are shown in Fig. 4 SM.

The planet's rotation rate exerts a fundamental control on the tide (Green et al., 2019) by setting resonant periods. Increasing Earth's current rotation rate to 3 hours also means the number of semi-diurnal periods in one present day Earth day rises from 2 to 8, thereby potentially increasing the energy dissipation over a certain fixed period of time. This is indeed the case in the simulations herein, with dissipation enhanced in each example, setting an upper bound on the scatter. The large increases for maps G and F reflect the contribution of several smaller, resonant basins. With an 8 day day-length, dissipation is reduced across all configurations. Crucially, the influence of continental configuration is still apparent, with the rotation adjustment conforming to the upper and lower bounds of the scatter seen in Fig. 2a.

Our three frequency sensitivity simulations show, unsurprisingly, that dissipation changes when the frequency is changed due to change in the resonant properties of the basins. However, there is not necessarily a continuous trend in the results, nor can we state if we have hit maximum global resonance in terms of rotation. For very fast or slow spin rates resonances become more localised and will not contribute to globally integrated dissipation rates to the same extent as at more moderate rates – see Green et al. (2019) for a discussion.

3.3 An influence on the rotational evolution

The slowing of the planets rotation rate is tied to the magnitude of tidal dissipation. In Table 1 we give an estimate of the variability introduced in the day-length, δLOD, as a function of just the M_2 frequency after 10^6 years. Eccentricity (e) and obliquity are 0, and we make the assumption that $de/dt = 0$. From conservation of energy and momentum, for a small moon orbiting a rapidly rotating planet such as the Earth-Moon system, the globally integrated dissipation, D, is related to the evolution of the Earth-Moon separation, a, as:

$$D = \frac{1}{2} a n \mathrm{M_M} (\omega - n) \frac{da}{dt} \tag{5}$$

where $\mathrm{M_M}$ is the Moon's mass (7.347×10^{22} kg), ω is the Earth's angular rotation rate, a is the Earth-Moon separation, $n = \sqrt{G(\mathrm{M_E} + \mathrm{M_M})/a^3}$ is the mean motion of the Moon ($G = 6.674 \times 10^{-11}$ m^3 kg^{-1}s^{-2} is the gravitational constant and $\mathrm{M_E} = 5.972 \times 10^{24}$

Table 1. Shown are the bathtub and topographic example dissipation rates (D_{BT} and D_{BY}) and the implications for the rotation rate, δLOD/Ma is the increase in day-length per 10^6 years relative to the present day-length.

Configuration	D_{BT} (TW)	D_{BY} (TW)	δLOD_{BT}/Ma (s)	δLOD_{BY}/Ma (s)
A	0.002	0.266	-0.013	-1.771
B	0.008	1.210	-0.053	-8.054
C	0.030	0.921	-0.200	-6.131
D	0.023	0.296	-0.153	-1.970
E	1.930	0.363	-12.847	-2.416
F	0.585	0.642	-3.894	-4.273
G	0.006	0.134	-0.040	-0.892
H	0.167	0.121	-1.112	-0.805

kg is Earth's mass). The angular deceleration, $d\omega/dt$, is related to D as:

$$D = -I(\omega - n)\frac{d\omega}{dt} \tag{6}$$

in which I is the rotating Earth's moment of inertia (8.04×10^{37}kg m^{-2}). An alternative method is given by MacDonald (1964). It is reasonable to assume that the values computed here and shown in Table 1 are underestimated by up to an order of magnitude because of the relatively coarse resolution used in our model. An elevated dissipation of course leads to an increased δLOD and the linear dependence clearly shows the importance of particular geologic features as the values in Table 1 do not consider shelf seas. Alone, the real deep ocean dissipation (0.9TW) gives a δLOD of 5.1s from Eq. 6 over a million years, the total real integrated dissipation (3.6TW) gives 24s, or for just M_2, 16s. Our simulation without shelf seas slows by ∼5s, compared to 42s for the full bathymetry, illustrating the outsized effect of shallow water energy losses on the planet's rotational evolution.

4 Discussion

Continental configuration complexity matters in discussions of a planet's tide because, for any given Earth-like planet, increasing the number of basins and/or embayment type features will increase the probability of resonant amplification. Furthermore, increasing the complexity of coastlines generates further energy loss due to acceleration around peninsula-type features. Numerical simulations have been used to test the effect of Earth's former continental configurations and bathymetry on the tide (Bjerrum et al., 2001; Green et al., 2017); however, to our knowledge there are no studies attempting to test a general influence of continental complexity on the ocean tide. This is difficult to do rigorously, given the problems in classifying complex non-Euclidean surfaces such as realistic continents, shapes that were once described as 'monstrosities' (Mandelbrot, 1982).

Our results put a constraint on the rotational evolution of planets with oceans and are of use for exoplanet estimates and deep time Earth tidal simulations alike. They also highlight the fundamental effect topography has on ocean tides: even with a few small continents or ocean bathymetry the dissipation can deviate by an order of magnitude from the water world estimate. There is also a strong link between rotation rate and dissipation (Green et al., 2019), and exoplanet rotation is currently difficult to determine from observation. With an equilibrium tide, Kepler-22b (initial rotation period of 1 Day) would have a rotation rate of about 2 Earth days after a 4.5Gyrs, while Proxima Centauri b (initial rotation period of 1 Day) would experience a rotation rate of some 12 days

(Barnes, 2017). We have shown that even with simple coastlines and a lack of bathymetry, the spin down could vary with an order of magnitude, and be order(s) of magnitude larger than in the equilibrium case.

As the continents aggregate and disperse during the 400–500Ma-long, super-continent cycle (Matthews et al., 2016), the tides become anomalously energetic during periods when the basins meet the conditions for resonance. A feature of this tectonically driven super-tidal cycle (Green et al., 2018) is a much less energetic tide during super-continental periods and a brief, more energetic state, for a few 10 Ma in between the subcontinents (Gotlib & Kagan, 1985; Green et al., 2017). The trend for more complex configurations to be more energetic in our results is analogous to this process and the tectonic setting thus exerts a first order control on the tidal dissipation. For example, the basin configurations in Figure 2E and G are qualitatively similar, yet E is substantially more dissipative due to its resonant state, whereas the large meridional continent in G blocks the tide. Equally, the range of the dissipation scatter at any point along the complexity scale (R) is roughly an order of magnitude (see Fig. 2a), which is comparable to the super-tidal fluctuation. Higher R-values tend to elevate dissipation, but not indefinitely. As continent size increases, a threshold must be reached where ocean area declines and suppresses dissipation. This is a key geologic control on the rotational evolution (see Table 1).

Earth's earliest continental crust is considered to have mostly formed between 3–2.5Ga (Korenaga, 2013, 2018), although this is debated. These early landmasses were probably small (Goodwin, 1996; Scotese, 2004): estimates for the Late-Archean suggest that $\sim$ 12% of Earth's surface area was continental crust, with only 2–3% as emerged land (Flament et al., 2008). This is compared to 42.5% of the surface being continental crust today, of which 27.5% is emerged land area (Schubert & Reymer, 1985; Flament et al., 2008; Cawood et al., 2013). In the micro-continental configurations in Fig 1A–C, a small semi-diurnal tide would be expected, even with the shorter tidal period and day-length at the time (Spalding & Fischer, 2019), but they still elevate the global dissipation by nearly an order of magnitude above the equilibrium tide (Fig 2a). However, this is still two orders of magnitude smaller than in simulations with larger, more numerous landmasses that generate more complex basins. It is likely that while Earth had a tidal dissipation rate much greater than the equilibrium tide early on in its history, it may have become more energetic with the formation of larger continents. However this result is not a model for an Archean tide; as shown, shelf-sea area and deep-ocean bathymetry, both unknown for the period, would be key controls.

The amount of energy dissipated in our simulations suggests an upper limit near 1.9TW for the deep ocean dissipation, given the similarity between the simulations with and without bathymetry. If the overestimation due to our coarse resolution is considered, a value of $\sim$0.76TW may be more realistic, supported by the dissipation value produced without shelf seas (Fig 2). These values do of course depend upon the topographic properties: even with a randomised bathymetry the influence of continental configuration is clear, but is not necessarily a good predictor of the tidal dissipation. Also, the smallest bathymetric features in our grids are of the order of $\sim$ 100km horizontally, and are of a higher relief than the Earth grid. Grid A for example possesses a canyon many thousands of kilometres long. Given the nonlinear dependence on bathymetric slope in Eq. 4), it is possible that the conversion fraction is overestimated, but this is an avenue for future work.

The broader implication for Earth-like exoplanets is that while an ocean may raise global tidal dissipation rates, a basin (or basins) with time-varying dimensions due to tectonics will, in a similar fashion to Earth, cause this value to fluctuate considerably over the planet's history. We suggest that it could span three orders of magnitude solely due to continental configuration. Planets with complex ocean bathymetry are likely to have larger tidal dissipation rates, and hence spin down much quicker, than more bath-

tub like oceans. The apparent convergence generated by adding the SMD bathymetry is an argument for including even a randomised ocean floor in planetary tidal models.

The tidal modulation by Earth's tectonics gives these results a robust standard to compare against, but the complexity metric may also have implications for Earth's early history, for periods with limited records of continental position and size.

Acknowledgments

Torben Morgensen's advice on the use of the map generator is acknowledged. The simulations were done on Supercomputing Wales, and their support is greatly appreciated. This work was supported by the NASA Astrobiology Program through collaborations arising from our participation in the Nexus for Exoplanet System Science, and by the NASA Planetary Atmospheres Program. RB acknowledges support from NASA grant NNX15AN35G. MJW is thankful for support from the Goddard Space Flight Center's Sellers Exoplanet Environments Collaboration (SEEC), which is funded by the NASA Planetary Science Division's Internal Scientist Funding Model, and the NASA Habitable Worlds Program. The data can be downloaded from the Open Science Framework (https://osf.io/p7ay9/). Constructive comments from two anonymous reviewers greatly improved the manuscript.

References

Balbus, S. A. (2014). Dynamical, biological and anthropic consequences of equal lunar and solar angular radii. *Proceedings of the Royal Society A: Mathematical, Physical and Engineering Sciences*, *470*(2168). doi: 10.1098/rspa.2014.0263

Barnes, R. (2017). Tidal locking of habitable exoplanets. *Celestial Mechanics and Dynamical Astronomy*, *129*(4), 509–536.

Batalha, N. M., Rowe, J. F., Bryson, S. T., Barclay, T., Burke, C. J., Caldwell, D. A., ... Welsh, W. F. (2013). Planetary candidates observed by kepler. III. Analysis of the first 16 months of data. *Astrophysical Journal, Supplement Series*, *204*(2), 1–13. doi: 10.1088/0067-0049/204/2/24

Bills, B. G., & Ray, R. D. (1999). Lunar orbital evolution: A synthesis of recent results. *Geophysical Research Letters*, *26*(19), 3045–3048.

Bjerrum, C. J., Surlyk, F., Callomon, J. H., & Slingerland, R. L. (2001). Numerical paleoceanographic study of the early Jurassic transcontinental Laurasian Seaway. *Paleoceanography*, *16*(4), 390–404.

Boué, G., & Efroimsky, M. (2019, Jul). Tidal evolution of the Keplerian elements. *Celestial Mechanics and Dynamical Astronomy*, *131*(7), 30. doi: 10.1007/s10569-019-9908-2

Cassan, A., Kubas, D., Beaulieu, J. P., Dominik, M., Horne, K., Greenhill, J., ... Wyrzykowski, L. (2012). One or more bound planets per Milky Way star from microlensing observations. *Nature*, *481*(7380), 167–169. doi: 10.1038/nature10684

Cawood, P. A., Hawkesworth, C. J., Dhuime, B. (2013). The continental record and the generation of continental crust. *GSA Bulletin*, *125*(1-2), 14–32. doi: /10.1130/B30722.1

Colose, C. M., Del Genio, A. D., & Way, M. J. (2019, May). Enhanced Habitability on High Obliquity Bodies near the Outer Edge of the Habitable Zone of Sun-like Stars. *arXiv e-prints*, arXiv:1905.09398.

Darwin, G. H. (1899). *The tides and kindred phenomena in the solar system.* Houghton, Boston.

Dickey, J. O., Bender, P. L., Faller, J. E., Newhall, X. X., Ricklefs, R. L., Ries, J. G., ... Yoder, C. F. (1994, 7). Lunar Laser Ranging: A Continuing Legacy of the Apollo Program. *Science*, *265*(5171), 482 - 490.

Dressing, C. D., & Charbonneau, D. (2015). the Occurrence of Potentially Habitable Planets Orbiting M Dwarfs Estimated From the Full Kepler Dataset and an

Empirical Measurement of the Detection Sensitivity. *Astrophysical Journal*, *807*(1), 45.

Dressing, C. D., Charbonneau, D., Dumusque, X., Gettel, S., Pepe, F., Collier Cameron, A., ... Watson, C. (2015). The mass of kepler-93b and the composition of terrestrial planets. *Astrophysical Journal*, *800*(2).

Egbert, G. D., & Ray, R. D. (2001). Estimates of M2 tidal energy dissipation from TOPEX/Poseidon altimeter data. *Journal of Geophysical Research C: Oceans*, *106*(C10), 22475–22502. doi: 10.1029/2000JC000699

Egbert, G. D., Ray, R. D., & Bills, B. G. (2004). Numerical modeling of the global semidiurnal tide in the present day and in the last glacial maximum. *Journal of Geophysical Research: Oceans*, *109*(C3).

Ferraz-Mello, S., Rodríguez, A., & Hussmann, H. (2008, May). Tidal friction in close-in satellites and exoplanets: The Darwin theory re-visited. *Celestial Mechanics and Dynamical Astronomy*, *101*, 171-201.

Flament, N., Coltice, N., & Rey, P. F. (2008). A case for late-Archaean continental emergence from thermal evolution models and hypsometry. *Earth and Planetary Science Letters*, *275*(3-4), 326–336.

Fressin, F., Torres, G., Charbonneau, D., Bryson, S. T., Christiansen, J., Dressing, C. D., ... Batalha, N. M. (2013). The false positive rate of Kepler and the occurrence of planets. *Astrophysical Journal*, *766*(2).

Goodchild, M. F., & Mark, D. M. (1987, 6). The Fractal Nature of Geographic Phenomena. *Annals of the Association of American Geographers*, *77*(2), 265–278.

Goodwin, A. M. (1996). *Principles of Precambrian geology* Elsevier.

Gotlib, V. Y., & Kagan, B. A. (1985). A reconstruction of the tides in the paleocean: Results of a numerical simulation. *Deutsche Hydrographische Zeitschrift*, *38*(2), 43–67.

Green, J., Way, M., & Barnes, R. (2019). Consequences of Tidal Dissipation in a Putative Venusian Ocean. *The Astrophysical Journal*, *876*(2), L22.

Green, J. A. M., Huber, M., Waltham, D., Buzan, J., & Wells, M. (2017). Explicitly modelled deep-time tidal dissipation and its implication for lunar history. *Earth and Planetary Science Letters*, *461*, 46–53. doi: 10.1016/j.epsl.2016.12.038

Green, J. A. M., Molloy, J. L., Davies, H. S., & Duarte, J. C. (2018). Is there a tectonically driven supertidal cycle? *Geophysical Research Letters*, *45*, 3568–3576. doi: 10.1002/2017GL076695

Green, J. A. M., Way, M. J., & Barnes, R. (2019). Consequences of tidal dissipation in a putative venusian ocean. *The Astrophysical Journal Letters*, *876*, 409-447. doi: 10.3847/2041-8213/ab133b

Hickman, A. E., Moore, C. M., Sharples, J., Lucas, M. I., Tilstone, G. H., Krivtsov, V., & Holligan, P. M. (2012). Primary production and nitrate uptake within the seasonal thermocline of a stratified shelf sea. *Marine Ecology Progress Series*, *463*, 39–57. doi: 10.3354/meps09836

Howard, A. W. (2013). Observed properties of extrasolar planets. *Science*, *340*(6132), 572–576.

Kagan, B. (1997). Earth-Moon tidal evolution: Model results and observational evidence. *Progress in Oceanography*, *40*(1-4), 109–124.

Kasting, J. F., Whitmire, D. P., & Reynolds, R. T. (1993). Habitable Zones around Main Sequence Stars. *Icarus*, *101*(1), 108–128.

Kopparapu, R. K., Ramirez, R., Kasting, J. F., Eymet, V., Robinson, T. D., Mahadevan, S., ... Deshpande, R. (2013). Habitable zones around main-sequence stars: New estimates. *The Astrophysical Journal*, *765*(2).

Korenaga, J. (2013). Initiation and evolution of plate tectonics on earth: Theories and observations. *The Annual Review of Earth and Planetary Sciences*, *41*.

Korenaga, J. (2018). Estimating the formation age of distribution of continental crust by unmixing zircon ages. *Earth and Planetary Science Letters*, *482*, 388–

395.

Kuhlbrodt, T., Griesel, A., Montoya, M., Levermann, A., & Rahmstorf, S. (2007). On the driving processes of the atlantic meridional circulation. *Reviews of Geophysics*, *45*. doi: 10.1029/2004RG000166

Leconte, J., Chabrier, G., Baraffe, I., & Levrard, B. (2010, June). Is tidal heating sufficient to explain bloated exoplanets? Consistent calculations accounting for finite initial eccentricity. *Astro. & Astrophys.*, *516*, A64+.

Lingam, M., & Loeb, A. (2018, 7). Implications of Tides for Life on Exoplanets. *Astrobiology*, *18*(7), 967–982.

MacDonald, G. J. F. (1964, 8). Tidal friction. *Reviews of Geophysics*, *2*(3), 467–541.

Mandelbrot, B. B. (1982). *The fractal geometry of nature* (Vol. 2). New York: WH freeman New York.

Matthews, K. J., Maloney, K. T., Zahirovic, S., Williams, S. E., Seton, M., & Muller, R. D. (2016). Global plate boundary evolution and kinematics since the late Paleozoic. *Global and Planetary Change*, *146*, 226–250.

Munk, W. (1968). Once again - tidal friction. *Quarterly Journal of the Royal Astronomical Society*, *9*(4), 352–375.

Munk, W. H. (1966). Abyssal recipes. *Deep-Sea Research and Oceanographic Abstracts*, *13*(4), 707–730.

Ray, R. D. (1997). Ocean self-attraction and loading in numerical tidal models. *Marine Geodesy*, *21*, 181-192.

Ray, R. D., Eanest, R. J., & Chao, B. F. (1996). Detection of tidal dissipation in the solid earth by satellite tracking and altimetry. *Nature*, *381*, 595-597.

Renaud, J. P., & Henning, W. G. (2017). Increased Tidal Dissipation Using Advanced Rheological Models: Implications for Io and Tidally Active Exoplanets. *The Astrophysical Journal*, *857*(2), 98.

Schubert, G., & Reymer, A. P. S. (1985). Continental volume and freeboard through geological time. *Nature*, *316*(6026), 336–339.

Scotese, C. (2004). A Continental Drift Flipbook. *The Journal of Geology*, *112*(6), 729–741.

Seager, S. (2013, 5). Exoplanet Habitability. *Science*, *340*(6132), 577 LP - 581.

Simpson, J. H., Brown, J., G., Matthews, J., & Allen, G. (1990). Tidal straining, density currents and stirring in the control of estuarine stratification. *Estuaries and Coasts*, *13*, 125-132. doi: 10.2307/1351581

Spalding, C., & Fischer, W. W. (2019). A shorter Archean day-length biases interpretations of the early Earth's climate. *Earth and Planetary Science Letters*, *514*, 28–36.

Srokosz, M., Baringer, M., Bryden, H., Cunningham, S., Delworth, T., Lozier, S., ... Sutton, R. (2012, 3). Past, Present, and Future Changes in the Atlantic Meridional Overturning Circulation. *Bulletin of the American Meteorological Society*, *93*(11), 1663–1676.

Stammer, D., Ray, R. D., Andersen, O. B., Arbic, B. K., Bosch, W., Carrère, L., ... Yi, Y. (2014). Accuracy assessment of global barotropic ocean tide models. *Reviews of Geophysics*, *52*(3), 243–282.

Taylor, G. I. (1920). Tidal friction in the irish sea. *Proceedings of the Royal Society of London series A*, *96*, doi: 10.1098/rspa.1919.0059.

Tsiaras, A., Waldmann, I. P., Tinetti, G., Tennyson, J., & Yurchenko, S. N. (2019). Water vapour in the atmosphere of the habitable-zone eight-earth-mass planet k2-18 b. *Nature Astronomy*. doi: 10.1038/s41550-019-0878-9

Tuerena, R. E., Williams, R. G., Mahaffey, C., Vic, C., Green, J. A. M., Naveira-Garabato, A., ... Sharples, J. (2019). Internal tides drive nutrient fluxes into the deep chlorophyll maximum over mid-ocean ridges. *Global Biogeochemical Cycles*, *33*, 995-1009.

Way, M. J., Del Genio, A. D., Aleinov, I., Clune, T. L., Robinson, T. D., Kelly, M.,

& Kiang, N. Y. (2018). Climates of warm earth-like planets. i. 3d model simulations. *The Astrophysical Journal Supplement Series*, *239*(2).

Way, M. J., Genio, A. D. D., Kiang, N. Y., Sohl, L. E., Grinspoon, D. H., Aleinov, I., ... Al, W. A. Y. E. T. (2016). Was Venus the first habitable world of our solar system? *Geophysical Research Letters*, *43*, 8376-8383.

Way, M. J., & Georgakarakos, N. (2017, Jan). Effects of Variable Eccentricity on the Climate of an Earth-like World. *Astrophysical Journal Letters*, *835*(1), L1. doi: 10.3847/2041-8213/835/1/L1

Way, M. J., & Del Genio, N. (2019, Dec). Venusian Habitable Climate Scenarios: Modeling Venus through time and applications to slowly rotating Venus-Like Exoplanets. *Journal of Geophysical Research: Planets*. doi: 10.1029/2019JE006276

Williams, D. M., & Pollard, D. (2002, Jan). Earth-like worlds on eccentric orbits: excursions beyond the habitable zone. *International Journal of Astrobiology*, *1*, 61-69. doi: 10.1017/S1473550402001064

Williams, D. M., & Pollard, D. (2003, Jan). Extraordinary climates of Earth-like planets: three-dimensional climate simulations at extreme obliquity. *International Journal of Astrobiology*, *2*(1), 1-19. doi: 10.1017/S1473550403001356

Williams, G. J., Sandin, S. A., Zgliczynski, B. J., Fox, M. D., Gove, J. M., Rogers, J. S., ... Smith, J. E. (2018). Biophysical drivers of coral trophic depth zonation. *Marine Biology*, *165*(4), 60.

Williams, J. G., Sinclair, W. S., & Yoder, C. F. (1978). Tidal acceleration of the moon. *Geophysical Research Letters*, *5*(11). doi: 10.1029/GL005i011p00943

Wilmes, S.-B., Green, J. A. M., Gomez, N., Rippeth, T. P., & Lau, H. (2017). Global Tidal Impacts of Large-Scale Ice-Sheet Collapses. *Journal of Geophysical Research: Oceans*, 1–17.

Wunsch, C., & Ferrari, R. (2004). Vertical mixing, energy, and the general circulation of the oceans. *Annual Review of Fluid Mechanics*, *36*(1), 281–314.

Yang, J., Boué, G., Fabrycky, D. C., & Abbot, D. S. (2014). Strong dependence of the inner edge of the habitable zone on planetary rotation rate. *Astrophysical Journal Letters*, *787*(1).

Zaron, E. D., & Egbert, G. D. (2006). Estimating Open-Ocean Barotropic Tidal Dissipation: The Hawaiian Ridge. *Journal of Physical Oceanography*, *36*(6), 1019–1035.